Implications on large-scale flow of the fractured EGS reservoir Soultz inferred from hydraulic data and tracer experiments

Name of authors:

Egert, Robert[a*]; Gholami Korzani, Maziar[a]; Held, Sebastian[a]; Kohl, Thomas[a]

E-Mail addresses:

robert.egert@kit.edu, m.gholami@kit.edu, sebastian.held@kit.edu, thomas.kohl@kit.edu

Addresses:

[a]Institute of Applied Geosciences, Karlsruhe Institute of Technology, Adenauerring 20b, 76131 Karlsruhe, Germany

Implications on large-scale flow of the fractured EGS reservoir Soultz inferred from hydraulic data and tracer experiments

Egert, Robert; Gholami Korzani, Maziar; Held, Sebastian; Kohl, Thomas

Abstract

The Enhanced geothermal system in Soultz-sous-Forêts, located in the geothermal favorable Upper Rhine Graben, is a fracture-controlled reservoir that was highly investigated in the last decades generating a huge geoscientific database. Numerical reservoir models use this database to simulate the operation of the subsurface heat exchanger, yet suffer from simplifications regarding the transfer of experimental into model data, dimensional extension, and computational power and efficiency. The new extensive transient 3-D simulations, based on geophysical, geological and hydraulic data, highlight the hydraulic and transport feedback of the Soultz EGS due to convective and advective fluid flow. Developed with the goal of simulating the vast tracer test data during the reservoir-testing phase in 2005, the Finite Element Model is focusing on the main fractured zones, which connect the wells in the deep reservoir. It comprises 13 major hydraulically active faults and fractures in a 13x11x5 km extending model domain, as well as open-hole sections of the wells GPK1 to GPK4 and their casing leakages. The simulation of the tracer experiment confirms the strong heterogeneity of the reservoir and highlights the importance of a potential fractured zone, hydraulically separating the reservoir in a northern (GPK1 to 3) and southern section (GPK4). This zone tends to connect the reservoir to the main fault system by hydraulically separating GPK4 from the other wells. The calibration and sensitivity analyses provide a unique, broad understanding of the reservoir flow zones providing information on the extension of the Soultz reservoir in the future and on the fluid pathways in the deep subsurface of the Upper Rhine Graben.

Keywords

Enhanced Geothermal System; Soultz-sous-Forêts; Discrete Fracture Network; tracer experiment; Finite Element, transport modeling

1. Introduction

The Upper Rhine Graben (URG) is one of the most distinct areas in central Europe for the utilization of geothermal energy. Favorable thermal conditions with gradients of greater than 100 $K.km^{-1}$ (Pribnow and Schellschmidt, 2000) have led to the development of several successful power plant projects targeting the hydrothermal sedimentary cover and the deep crystalline basement of the URG as Enhanced Geothermal System (EGS) (Genter et al., 2016; Vidal and Genter, 2018). EGS are designed to take advantage of natural permeable faults and fractures and improve their natural

hydraulic properties through chemical and hydraulic stimulation (Schindler et al., 2010). One of the first and most prominent European EGS is located at Soultz-sous-Forêts (Garnish, 2002; Gérard et al., 2006), targeting a fractured geothermal reservoir in a depth of up to 5000 m and temperatures up to 200 °C (Genter et al. 2010). Starting in the 1980s, a unique scientific database has been created, which opens the opportunity to study hydraulic processes in the geothermal reservoir, and especially along faults and fractures and on the matrix-fracture-interface (Genter et al., 2010; Sausse et al., 2010).

Various experiments, such as tracer and circulations tests, were conducted to characterize and quantify fluid flow through a single fracture or fracture networks not only in the Soultz EGS but in laboratory and field experiments worldwide (Berkowitz, 2002). In laboratory scale, single fracture geometries were often described as self-affine rough surfaces with varying apertures exposed to laminar and/or turbulent fluid flow (Schmittbuhl et al., 2008). Meter-scale migration experiments, conducted in Underground Research Laboratories, considered fractures as shear zones with a high number of small discrete channels (Hadermann and Heer, 1996). Typically, Darcy flow was assumed within the shear zone (Moreno et al., 1988). In the reservoir scale, the geometry, interconnection, and behavior of fractures are sparsely known and accessible since wellbores and experiments provide point-like information of shape and fracture density (Dezayes et al., 2010) while geophysical measurements show the spatial distribution (Sausse et al., 2010). Detailed information about the reservoir hydraulics, including the reservoir fluid migration pathways, mean residence times, swept pore volume and heat exchange area between different wells, can be achieved using inter-well tracer experiments (Robinson and Tester, 1984). In the past, several tracer experiments were conducted in enhanced geothermal reservoirs which, however, were assumed to be simplified connections between two wells as a single planar structure or ideal fracture network when attempting to model (Ayling et al., 2016; Ghergut et al., 2016; Iglesias et al., 2015; Karmakar et al., 2016; Rose et al., 2009; Sanjuan et al., 2006).

An elegant way to resolve arisen issues of missing spatial information and unconnected data is to simultaneously apply structural and numerical models for investigating the natural and forced hydro-thermal processes of an EGS (O'Sullivan et al., 2001). Various numerical studies of the Soultz geothermal reservoir have been conducted over decades for investigating different physical processes, such as natural convection (Bächler et al., 2003; Guillou-Frottier et al., 2013; Kohl et al., 2000; Vallier et al., 2019) and the effects of mechanical stimulation to the reservoir performance (Baujard and Bruel, 2006; Kohl et al., 2006; Kohl and Mégel, 2007). Furthermore, inter-well circulation was investigated by fitting analytical and numerical solutions to the measured tracer data. Sanjuan et al. (2006) applied an analytical dispersive transfer model while Blumenthal et al. (2007) and Gessner et al. (2009) presented simplified models for the direct circulation between GPK3 and GPK2 wells. Kosack et al. (2011) compared three different inversion methods to evaluate their

applicability to the connection between GPK3 and GPK2. Vogt et al. (2012) applied the Ensemble Kalman Filter (EnKF) to individually invert for the concentrations measured at GPK2 and GPK4. Gentier et al. (2010; 2011) developed a first Discrete Fracture Network (DFN) considering hydraulically active parts and fracture sets and independently adapted the model for both wells using a particle tracking method. It was concluded that it is not possible to create a single homogeneous statistical fracture model that reproduces both wells simultaneously, as the main structure interferes with the hydraulic field between GPK3 and GPK4. Radilla et al. (2012) fitted a model to the experimental data, connecting the individual wells on three independent and isolated pathways with an equivalent stratified medium approach. All authors commonly conclude that a single-fracture approach is not suitable to sufficiently describe the hydraulic flow in the complex Soultz geothermal reservoir.

EGS are often simplified as theoretical/hypothetical fracture systems, connecting two wells along a line or one or more parallel plates (Bataillé et al., 2006; Fox et al., 2013; Vallier et al., 2019). It is known from the well-developed Soultz geothermal reservoir that this assumption does not adequately describe the structure of the heat exchanger system in an EGS (Genter et al., 2010). The understanding of the complex faults & fractures pattern and thus, on the tectonic history, preferential flow paths and hydrothermal circulations are crucial for the sustainable and safe design of a geothermal operation avoiding any artificially induced risks, like thermal breakthrough or induced seismicity (Zang et al., 2014). Therefore, the goal of the present study is a qualitative and quantitative evaluation of naturally and artificially induced fluid flow in a complex fractured geothermal reservoir to further investigate impacts of the considered limiting assumptions in the literature and better understand complex fluid circulation. Moreover, the knowledge gained allows the optimization of the design of future experiments and operation scenarios and the prediction of expected results (Kohl and Mégel, 2007).

Herein, we present an extensive numerical study including the large structural complexity of the Soultz fault and fracture network solving a transient fully-coupled Hydro-Solute (HS) transport simulation with the TIGER code. The three-dimensional flow field and tracer propagation in the Soultz geothermal reservoir are predicted and represent a major extension of an earlier approach by Held et al. (2014). The model includes the granitic basement as well as several hydraulically active faults and fractures as discrete surfaces and the open-hole sections of the wells as discrete line features. Long-term inter-well circulation tests are initially used to forward invert the hydraulic parameters of the fracture network while the hydraulic model is further recalibrated to reproduce the inter-wells tracer experiment (Sanjuan et al., 2006). The combination of the numerical approach with different kind of experimental data allows quantification and evaluation of the flow field inside the heat exchanger of the Soultz EGS and the identification of inter-well connections over the complex

fracture network. The numerical approach allows a detailed characterization of the subsurface heat exchanger with the possibility to recognize feasible features for future expansion.

2. The Soultz geothermal reservoir

The Soultz geothermal system is located in the French-side of the central URG, which is part of the "European Cenozoic Rift System" extending from southern France to the North Sea (Ziegler and Dèzes, 2005). The major tectonic feature of the Soultz reservoir is a horst structure uplifting the Soultz reservoir between Hermerswiller and Kutzenhausen fault, narrowing the Cenozoic and Mesozoic cover to a thickness of 1400 m (Aichholzer et al., 2016). The underlying crystalline basement is characterized as a low-permeable naturally fractured rock (Hooijkaas et al., 2006; Sausse and Genter, 2005) with an alteration-dependent rock matrix permeability ranging from 10^{-19} m² to 10^{-20} m² (Hettkamp et al., 1999). The existing fault- and fracture-system is a result of the tectonic history of the URG. The dominant fracture orientation (160 ±15°) is linked to the recent maximum horizontal stress orientation of 170 ±10° (Cornet et al., 2007; Evans et al., 1997). Other fracture sets are oriented with Rhenish (20 ±10°) and Hercynian (130 ±10°) orientation with a steep dip (>60°) to the west (Dezayes et al., 2010). The mean aperture is varying between 0.1 mm and 250 mm (Dezayes et al., 2010). Fractures oriented parallel to the main stress field tend to remain open and thus contain increased permeability (Cornet et al., 2007), while those perpendicular or orthogonal to the main stress field have the tendency to be sealed.

As shown in Fig. 1, the Soultz EGS can be divided into three sub-reservoirs (2000 m, 3500 m, and 5000 m) and utilized by four wells (GPK1 to GPK4) (Schill et al., 2017). The boreholes were drilled into the western flank of the Soultz horst structure. The GPK1 well targets the middle reservoir with a maximum depth of 3600 m while GPK2 to GPK4 were drilled over 5000 m depth to exploit the deeper crystalline reservoir (Genter et al., 2010). The lowest 500 - 700 m section of each borehole is not equipped with a casing and left completely open against the rock. The remaining part is cased with leakages reported for GPK2 and GPK4 (Pfender et al., 2006). The leakage of the well GPK2 at the depth of 3880 m connects GPK2 to the major fractured and altered zone GPK3-FZ4770 and thereon to the well GPK3 (Sausse et al., 2010). Jung et al. (2010) concluded a fluid loss of more than 16 % in the leakage of GPK2 measured with the brine displacement method. The three deep wells are aligned NNW-SSE with a lateral distance of 650 m in a depth of 5000 m while the distance between GPK1 and GPK2 is 450 m.

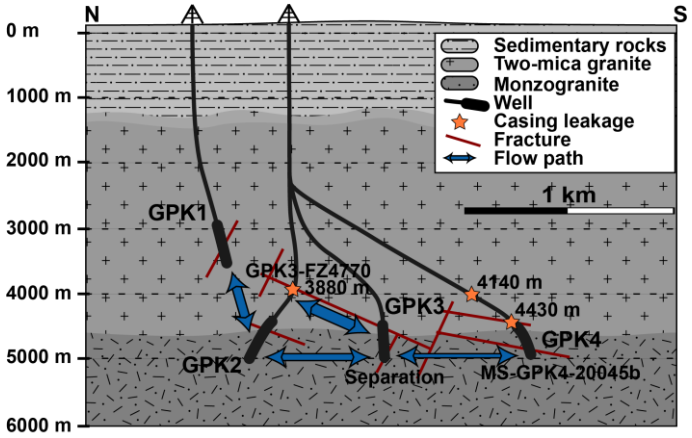

Fig. 1: 2D-Subset of the geological setting of the Soultz geothermal reservoir including wells, open-hole sections, and the considered lithological units. The main fractures are shown as red lines; the expected hydraulic connections based on Sanjuan et al. (2006) and Aquilina et al. (2004) are shown in blue; orange stars indicate the reported casing leakages

Circulation and inter-well tracer experiments allow the prediction of forced fluid flow and the hydraulic quantification of the connection between the individual wells, while spatial information, e.g. on the flow paths within the reservoir, is not known (Ghergut et al., 2013). At the Soultz site, several experiments have been conducted with different well setups during the long-term research activities (Schill et al., 2017). A tracer experiment carried out in 1997 examined the connection of GPK1 and GPK2 (Aquilina et al., 1998), while a tracer experiment in 2005 further focused on the main hydraulic connections in the deeper reservoir between GPK2, GPK3, and GPK4. Sanjuan et al. (2006) concluded two connections between GPK3 and GPK2 through a hydraulic short-circuit and an additional pathway of elevated length, while a poor link between GPK3 and GPK4 was observed. Further inter-well tracer experiments have been conducted confirming the main findings of this experiment (Sanjuan et al., 2015).

3. Numerical modeling

The numerical simulations are carried out with a Finite-Element (FE) open-source application called TIGER (THC sImulator for GEoscience Research) (Gholami Korzani et al., 2019), which is based on MOOSE (Multiphysics Object-Oriented Simulation Environment) framework (Gaston et al., 2009). TIGER has been developed to tackle thermo-hydraulic-solute transport problems in geothermal reservoirs including lower-dimensional features for fractures and well paths.

3.1. Governing equations

The approach assumes a Representative Elementary Volume (REV) for the porous media where interaction between the coupled processes can occur (Bear and Cheng, 2010). The hydraulic field is solved for the pore pressure by combining mass and momentum balances including Darcy's law (Bundschuh et al., 2010) as:

$$bS_m \frac{\partial P}{\partial t} + \nabla . b\boldsymbol{q} = Q \qquad \text{Eq. 1}$$

$$\boldsymbol{q} = \frac{\boldsymbol{k}}{\mu}\left(-\nabla P + \rho^{l}\boldsymbol{g}\right) \quad \text{Eq. 2}$$

where P is the pore pressure; t is the time; S_m is the mixture specific storage of the liquid and solid phase; Q is the source term for injection and production; k is the permeability tensor; μ is the fluid dynamic viscosity; ρ^{l} is the fluid density; **g** is the gravitational acceleration vector; **q** is the fluid or Darcy velocity vector and b is the scale factor for considering fractures (aperture) and wells (area). Lower-dimensional fractures are treated as discrete 2D elements while open-hole sections are discretized as 1D elements, sharing nodes, faces, and lines with the 3D continuum.

The transport of solutes (e.g. tracers) is considered as spatial and temporal changes of concentration which are governed by an advection-diffusion-dispersion equation (Bear and Cheng, 2010).

$$b\frac{\varphi\partial C}{\partial t} + b(-\nabla.\mathbf{D_m}\nabla C + \boldsymbol{q}\nabla.\mathrm{C}) = Q \quad \text{Eq. 3}$$

where C is the solute concentration; φ is the porosity; $\mathbf{D_m}$ is the sum of molecular diffusion and dispersion. The dispersion tensor is dependent on Darcy velocity and longitudinal and transversal dispersivity (Bear and Cheng, 2010), which generally describes the mixing around maximum concentration due to different mechanical effects (Bauget and Fourar, 2007).

3.2. Numerical model

A 3D-Discrete Fracture Matrix (DFM) model is used to ensure high accuracy in the geometrically complex reservoir by considering DFN and the surrounding matrix in the numerical analysis (Berre et al., 2018). The available information about the geological and tectonic settings, including well paths and open-hole sections, can be merged into a structural model of the Soultz geothermal reservoir. The used reservoir model, which is a subset of the structural model proposed by Sausse et al. (2010) and Place et al. (2011), is based on the 3D-model created by Held et al. (2014). However, the model is updated and extended in this study by introducing two additional fracture zones as 1) the WNW-ESE-oriented fracture “Separation” between the wells GPK3 and GPK4, and 2) GPK1-FZ2856 fracture intersecting GPK1 in the middle reservoir. The Separation fracture was not drilled but suspected as an anomalous zone of either higher permeability or hydraulic barrier, separating the deeper reservoir into a northern and a southern part (Calò et al., 2016; Kohl et al., 2006; Sausse et al., 2010). The fracture GPK1-FZ2856, identified using Vertical Seismic Profiling (Sausse et al., 2010), is added to allow better adjustment of hydraulic parameters close to the GPK1 well. The model has an extension of 13 (E-W) x 11 (N-S) km with a vertical depth of 5 km (Fig. 2), located between 1000 m and 6000 m below surface. The extension of the domain is chosen, to avoid boundary effects on the area of interest and to possibly consider the effects of the regional flow field. The minimum lateral distance between well and boundary is 4000 m.

Minor simplifications were made regarding the location, dipping and hydraulic appearance of the fracture network by representing fractures as discrete features. Out-of-plane mixing effects like

surface roughness, fault gauge or internal mixing cannot be treated individually and are therefore summarized in the hydrodynamic dispersion (Bauget and Fourar, 2007). Tsang et al. (1988) concluded that it is suitable to use a statistically homogenous system (e.g. for aperture, permeability) if the transport dimensions are significantly larger than the spacing between the channels belonging to a fracture and the transport distance is large enough to remain unaffected by local heterogeneities. The wells GPK1 to GPK4 are discretized over the entire open-hole section (and casing leakage) and connected with at least two fractures to the reservoir. The element size differs between 1.5 m (around and along the wells) and 500 m (close to the boundaries) with a typical element size around 40 m. As the fracture GPK3-FZ4770, establishing the main connection of GPK3 and GPK2 is inclined and not oriented parallel to the wells, the wells intersect the fracture in different reservoir levels resulting in the true distance of 840 m (compared to the often used 650 m derived from a pure horizontal distance). To consider the effects of hydraulic or chemical stimulation (Nami et al. 2008; Schill et al. 2017) and to minimize mesh dependency of the results, the main fracture GPK3-FZ4770 is subdivided and refined around GPK2 and GPK3. In total, the model contains 141'271 nodes which are connected by 714'453 elements including 3D matrix, 13 fractures, and 4 wells as shown in Fig. 2.

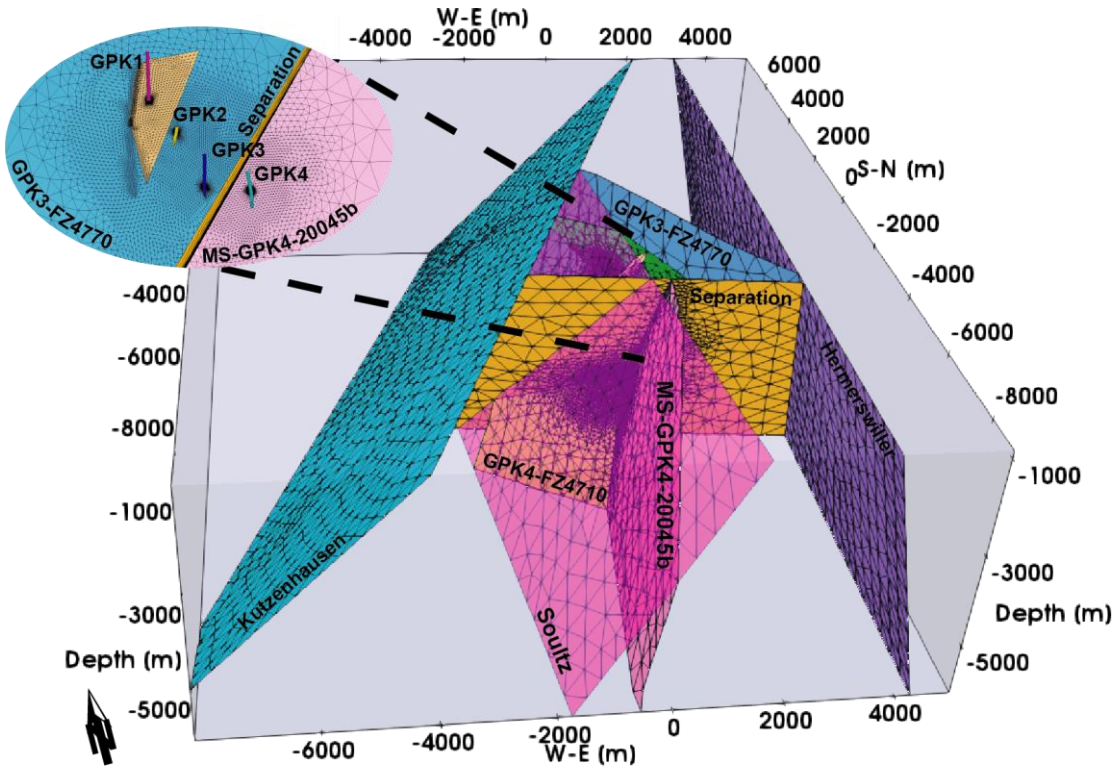

Fig. 2: 13-fracture-model of the Soultz geothermal reservoir including wells (modified after Held et al. (2014)). Grey shows the extension of the matrix. 10 out of 13 discrete faults and fractures are shown. The central area of the mesh along GPK3-FZ4770 and between GPK2, GPK3, and GPK4 is shown in detail.

The pore pressure in the whole reservoir is assumed to be hydrostatic (Stober and Bucher, 2007) by setting the top and bottom boundary conditions (BC) as Dirichlet BC and the model initial condition (IC) in accordance. Injection and extraction rates are applied as time-dependent mass-flux-function

on top of each open-hole section. The matrix permeability is assumed to be orthotropic with higher permeability in N-S-direction to take the regional stress field of the URG and small-scale fractures into account (Cornet et al., 2007). A natural S-N-oriented graben-parallel background flux of 1 $m^3.h^{-1}$ (Bächler et al., 2003; Sanjuan et al., 2006) is applied to the main faults and fractures as a function of the individual aperture.

The injected fluorescein tracer is assumed to be conservative in terms of reaction and sorption during transport as well as radioactive and thermal decays (Adams and Davis, 1991; Berkowitz, 2002). Solute diffusion, dispersion, and advection into the granitic basement are neglected (Bodin et al., 2003), as the porosity of the matrix is significantly smaller than the ones of the DFN (Aquilina et al., 2004). The solute (re-)injection is applied as time-dependent Dirichlet BC inferred from concentration measurements at GPK3 wellhead. The parametrization of the matrix and fluid properties took into account the conditions in the reservoir (e.g. increased temperature and salinity, Table 1). For enhancing the accuracy, minimizing unwanted numerical diffusion and conservation of the sharp concentration front, a second-order semi-implicit time-integration method (Crank and Nicolson, 1996) and a Streamline Upwind method (Brooks and Hughes, 1982) are applied.

Table 1: Constant model input parameters for the fluid and solid phases, the reservoir brine properties are in accordance with Kestin et al. (1981) representing a brine with 150 °C, 35 MPa and 1.5 mol.kg^{-1} salinity

Parameter	Value
Fluid density [kg.m^{-3}]	1065
Fluid dyn. viscosity [Pa.s]	2.3×10^{-4}
Fluid compressibility [Pa^{-1}]	2×10^{-9}
Matrix compressibility [Pa^{-1}]	5×10^{-13}
Fracture porosity [-]	1
Matrix porosity [-]	1×10^{-2}
Solute diffusion [m².s^{-1}]	4×10^{-10}

4. Results

4.1. Calibration of the hydraulic and solute processes

The transmissivities of the Soultz fracture network are calibrated against two circulation tests conducted in 2009 (Schindler, 2009) and 2011 (Genter et al., 2011). Flow rate changes at wellheads and their effects on the reservoir pore pressure were used to quantify the transmissivities of the faults and fractures. Flow velocity logs from each borehole were used to assign the measured portion of flux to the individual fractures since the matrix tends to have significantly lower permeability. The calibration is necessary because two further fractures, compared to Held et al. (2014), affect the pressure field and the capability of TIGER in applying time-dependent BCs enabling more accurate modeling of the reservoir.

A circulation test, with average flowrates between 9 and 20 l.s^{-1}, conducted in early 2011 (Genter et al., 2011) allowed the calibration of the fractures connected to three wells of GPK1, GPK2, and GPK3 through production in GPK2 and reinjection in GPK1 and GPK3. Fig. 3 shows the pore pressure changes at GPK1 to GPK3 after the calibration of the fractures' transmissivity. For GPK1, no flow rate data was recorded from 8th to 10th day of the experiment leading to no flow in the simulation. However, the pressure response almost fitted the measured data. The lower pressure increase in GPK1, compared to GPK3, indicates a good connection of the borehole to high permeable zones. For GPK2, the simulated data slightly underestimates the pressure response in the first 50 days, while it overestimates later. A casing leakage was reported after day 47 (Genter et al., 2011), affecting the experimental results. This leakage caused the fluid already pumped in the pipe to flow back into the reservoir and led to lower measured pressure change for the measured flow rates. That leakage was not incorporated in this study as it only affects the internal system of GPK2 well.

The measurements of GPK3 show high scattering up to 20 days, which was caused by strongly varying flow rates at the start of the experiment. After 20 days, the flow rate was kept constant, leading to a steady pressure change until the end of the experiment. The obtained pressure changes for GPK3 did not well match the measured data between day 5 and 15. The missing match could be the result of several factors like borehole or skin effects, (re-) opening of small-scale fractures, changes in the flow regime and leakages in the tubing. Since the proposed model focusses on long-term evaluation, the calibration was done by fitting the mean steady section of the experimental data. It is worthwhile noting that the injection wells (GPK1 and GPK3) have almost the same average flow rates (approx. 9 l.s^{-1}) and at the same time have significantly different pressure responses. The immediate pressure decline after the pump shutdown shows a small storage effect along the different fractures and the granitic matrix.

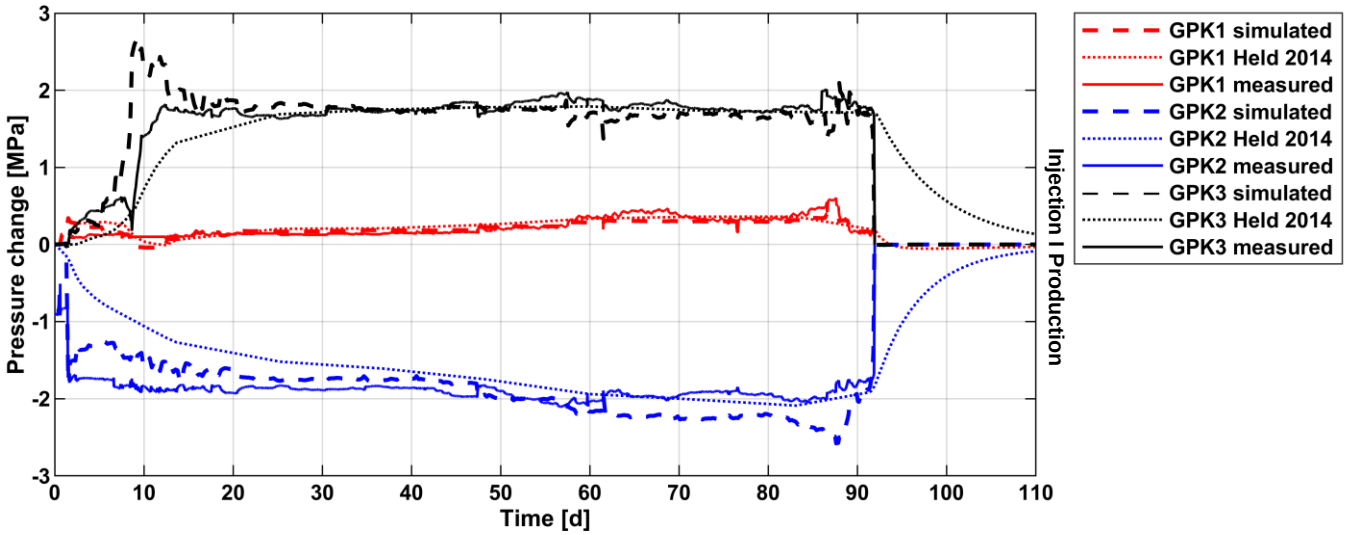

Fig. 3: Pressure changes in comparison with the measured data and results of Held et al. (2014). Positive pressure changes represent fluid injection.

A single-well circulation test in 2009 (Schindler, 2009) was used to calibrate the transmissivities of the fractures in the southeastern part of the reservoir connected to GPK4 (Fig. 4). Strongly varying flow rates up to the 10th day were only partially considered because their influence on the long-term reservoir behavior is negligible. Discrepancies between simulated and measured data occurring after 110 days are probably due to disturbances in the experimental sequence. Therefore, the steady pressure change between day 30 and 110 was used for the calibration of the hydraulic features.

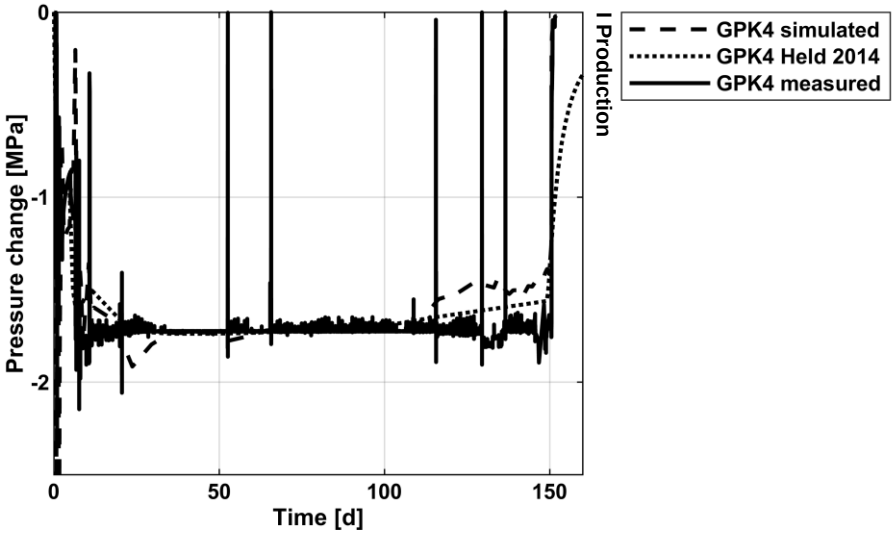

Fig. 4: Pressure changes compared with the measured data and results of Held et al. (2014) for GPK4. Missing experimental data leads to zero values.

The faults and fractures were calibrated for their transmissivities and the granitic matrix for the permeability and hydraulic diffusivity (Table 2). In comparison to Held et al. (2014), the calibrated data differs slightly. It is worthwhile noting that the fractures close to the wells affect the calibration results decisively. Therefore, the calibrated transmissivities have a high accuracy in the vicinity of the wells, but give only a rough estimate for the hydraulic properties of remote faults and fractures.

Table 2: Calibrated transmissivities of the faults and fracture network and the permeability of the matrix.

Name	Transmissivity [m².s^{-1}]			Permeability [m²]
GPK3-FZ4770	4.80E-05	**Granitic matrix**	**x**	1.34E-16
GPK1-FZ2856	5.00E-05		**y**	3.30E-16
GPK1-FZ2120	3.80E-04		**z**	1.65E-16
GPK3-FZ5020	1.68E-05			
GPK4-FZ4710	3.80E-05			
Soultz fault	6.80E-05			
Kutzenhausen fault	6.80E-04			
MS-GPK2-2000a	5.10E-05			
MS-GPK3-2003a	3.90E-04			
MS-GPK4-20045b	3.20E-05			
Hermerswiller fault	6.80E-05			
PS3-Int (VSP)	6.40E-04			
Separation	6.80E-05			

GPK3-FZ4770-GPK2	5.65E-05		
GPK3-FZ4770-GPK3	2.95E-05		

4.2. Flow field

The findings of the circulation experiments can be coupled to multi-well tracer experiments for quantifying the inter-well connection and flow field of the Soultz geothermal reservoir. A 145-day tracer test was carried out between July and December 2005 in the wells GPK2 to GPK4 (Sanjuan et al., 2006). During the experiment, fluorescein tracer was injected in GPK3 and extracted from GPK2 and GPK4. The fluid, extracted with average flow rates of 11.9 $l.s^{-1}$ (GPK2) and 3.1 $l.s^{-1}$ (GPK4), was reinjected in GPK3 with 15 $l.s^{-1}$. The fluorescein concentration during injection was 146 $mg.l^{-1}$ over 24 h. Before the first injection, 8 days of circulation provided a stationary flow field. The results of the experiment and best-fit modeling for the wells GPK2 and GPK4 are shown in Fig. 5 and Fig. 7. The peak velocities of the different pathways were fitted under the assumption of the obtained transmissivities in the previous section by adapting the permeability to the expected and measured travel time and fluid velocities along the affected fractures. The mixing around the breakthrough maximum was achieved by adjusting the longitudinal and transversal dispersivity and the variation of the aperture. In addition, the 95% confidence interval as the result of the standard error of the mean modeled solute concentration is presented.

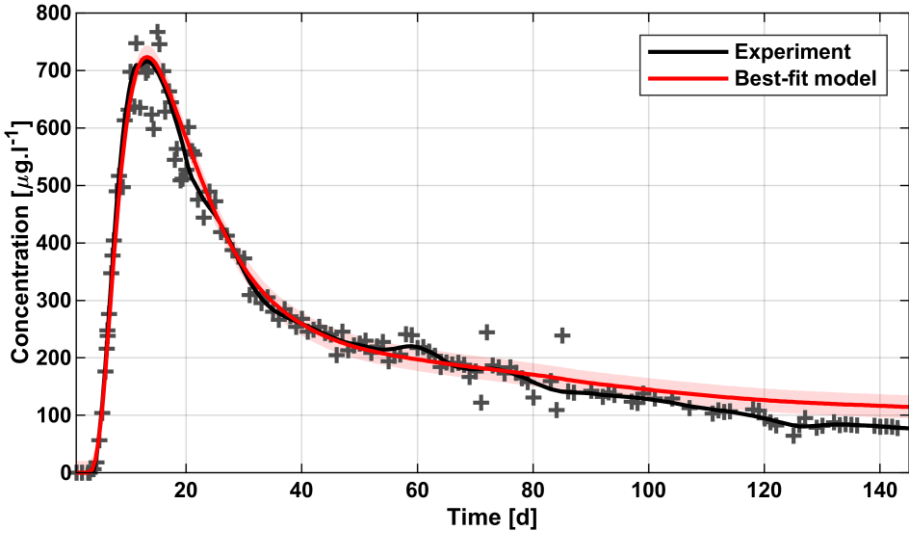

Fig. 5: Simulated and measured fluorescein concentration at well GPK2; The grey crosses are the experimental data, and the black line shows their mean value. The red line shows the best-fit model with a 95% confidence interval as the red shadow.

Fig. 5 shows the modeled and observed results of GPK2 for the tracer breakthrough curve (BTC). The maximum concentration (730 $\mu g.l^{-1}$), giving a peak velocity of 2.6 $m.h^{-1}$, was observed after 13 days. A strong tailing is noticeable until the end of the experiment, which could be the result of 1) diffusive exchange with matrix, 2) dispersive effects in the fracture channeling and/or 3) the interconnection of the wells by different fracture sets (Becker and Shapiro, 2000). As shown in Fig.

8 the tailing could be related to the latter option. It is possible to identify and quantify two to three different hydraulic pathways connecting GPK3 and GPK2 (Fig. 6). The main solute influx in GPK2 was identified to occur along the fracture GPK3-FZ4770, connecting the open-hole section of GPK3 with the casing leakage of GPK2. The entire amount of tracer along this pathway was swept after 90 days of circulation. The second pathway along GPK3-FZ4770 and MS-GPK2-2000a was noticed after 26 days and has a maximum concentration of 161 µg.l^{-1} after 90 days with a peak velocity of 0.5 m.h^{-1}. The third pathway, along GPK3-FZ5020 and MS-GPK2-2000a, shows a strong dilution with reservoir fluids, which is why no peak concentration can be detected in the simulation. The lower total measured concentration compared to the second pathway tracer concentration after 90 days (Fig. 6) can be explained by additional mixing along the well trajectory of GPK2. The mixing took place when the higher concentrated fluid, entering the open hole section of GPK2, passed the casing leakage on its way upwards and was mixed with the less concentrated fluid of the upper pathway. These pathways were also confirmed in further experiments conducted in 2010 and 2013 along this pathway (Sanjuan et al., 2015).

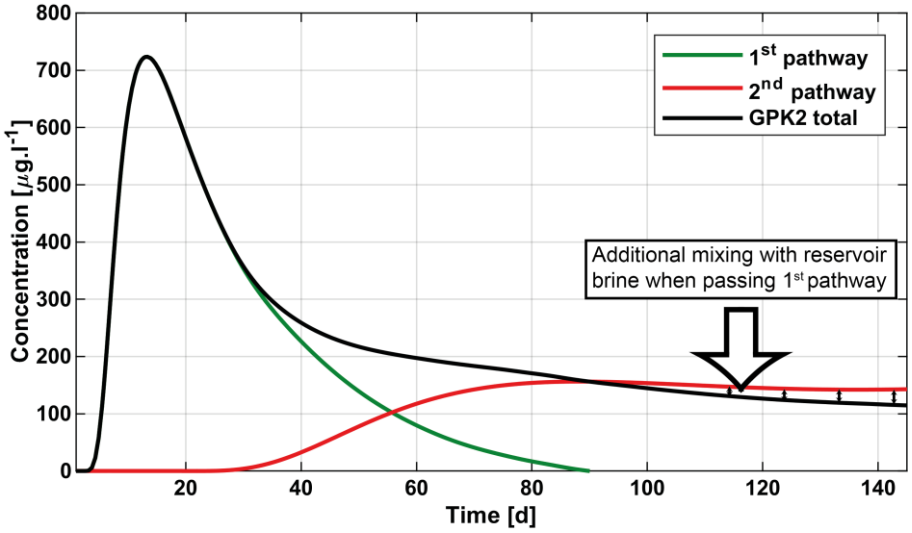

Fig. 6: Simulated tracer concentration at the GPK2 wellhead by showing the contributions of the individual pathways

The result of the simulation at GPK4 in comparison to the experimental data is shown in Fig. 7. The first arrival occurred 23 days after injection while the maximum concentration (31 µg.l^{-1}) was measured at the end of the experiment. A peak in the concentration, similar to the recorded one for GPK2, cannot be observed within the experimental period. The BTC shows typical behavior with clear mixing effects, such as strong dilution and no clear maximum. The reported scattered measured data could not be reproduced in the simulation. Predictions about the mean transfer time and maximum concentration are therefore subject to a high degree of uncertainty. Assuming a continuous circulation and constant flow rates, the peak concentration of 48 µg.l^{-1} was observed after 1.5 years followed by a decline to 23 µg.l^{-1} at the end of the long-term forecast (5 years) (Fig. 7b). The relatively late arrival time at GPK4 compared to GPK2 indicates the low fluid velocity (0.06 m.h^{-1}) of this pathway. Combined with the low tracer concentration and widely spread peak, a poor

hydraulic connection between both boreholes is clear probably due to the Separation fracture. The fracture is oriented in WNW-ESE-direction and thus acts as an anomalous zone, which hydraulically unlinks the two parts of the reservoir from each other by creating a preferential pathway and drainage along itself. Fig. 8 shows the dimensionless solute concentration on the affected faults and fractures at several time steps. The proposed different hydraulic pathways can be identified as areas with an increased solute concentration, which allow the movement of the solute between the injection and extraction wells.

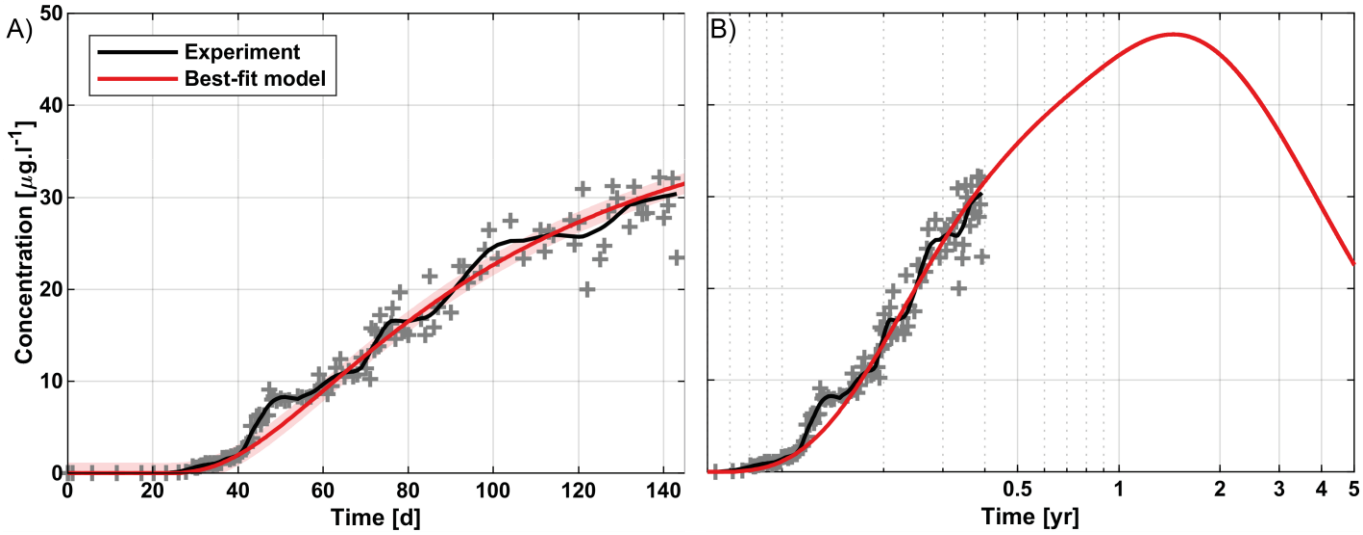

Fig. 7: Simulated and measured dimensionless fluorescein concentration at GPK4; A) over the experimental duration; B) long-term forecast for 5 years. The grey crosses are the experimental data, and the black line shows their mean value. The red line is the result of the best-fit model with a 95 % confidence interval as the red shadow.

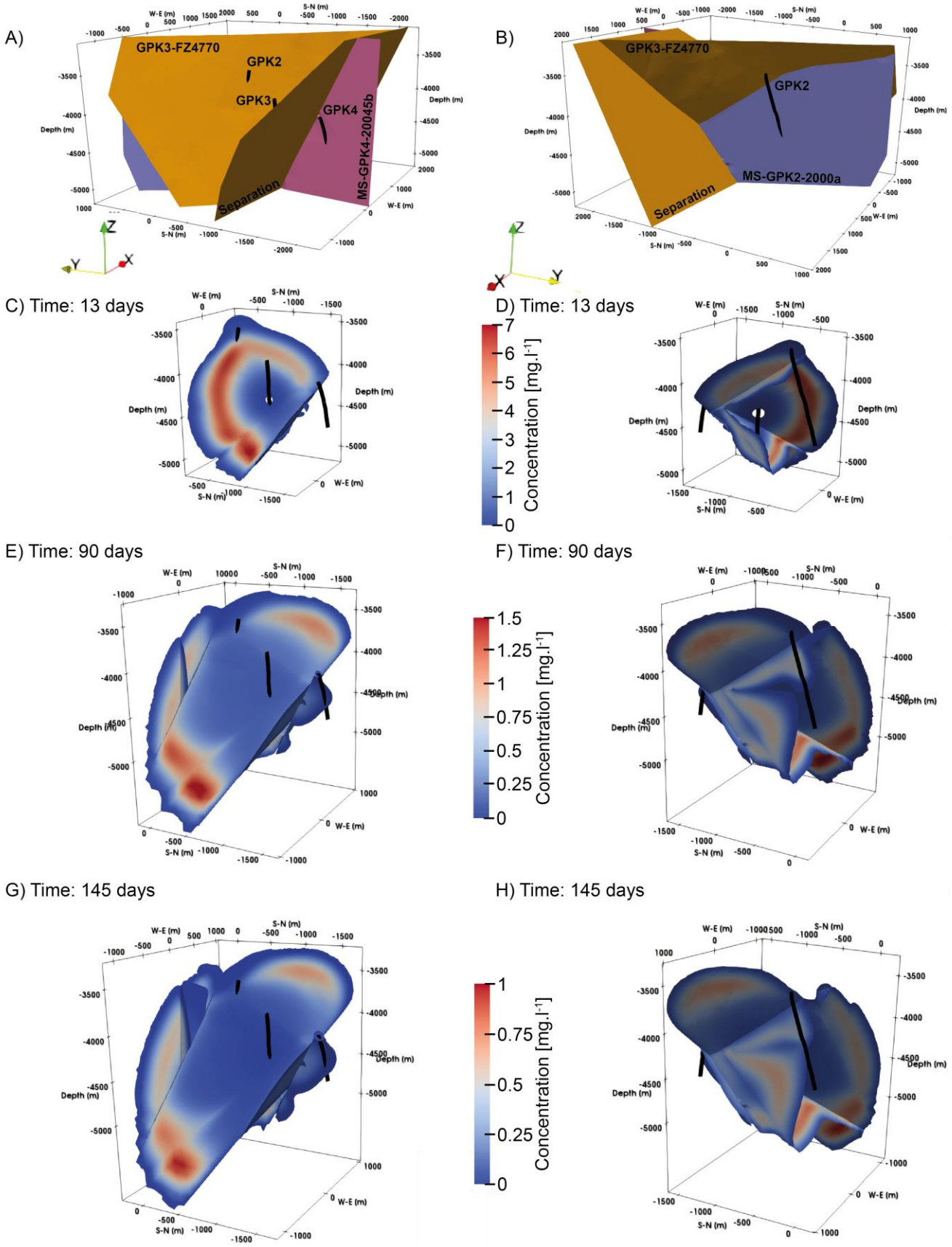

Fig. 8: Comparison of tracer concentrations in different faults and fractures. Left side) View from southwest, right side) View from the northeast. A-B) the mainly affected fractures, C-D) the tracer concentration at GPK2 reaches the maximum, E-F) the second pathway reaches the maximum and G-H) the end day of the experiment.

In addition to the hydraulic characterization of the DFN, effects of other factors, including tracer reinjection and background flux, which are of great importance for the (long-term) evaluation of the fracture network, were studied. The reinjection of the tracer-enriched produced fluid in GPK3 affected the evolution of long-term concentrations. After the arrival of the main peak, the reinjection of enriched fluids leads to elevated tracer concentrations along GPK3-FZ4770. At the end of the experiment period, Fig. 9a illustrates a 20 % reduction in the tracer concentration at GPK2 if the tracer reinjection was neglected. This factor influenced the concentration obtained for GPK4 less prominently than for GPK2 but a 6 % reduction is still documented in Fig. 9b.

Another factor is the effect of the natural background flux along the main faults and fractures due to the natural convective system of the Soultz reservoir. A minimum velocity of 11 cm.yr^{-1} reported by Vallier et al. (2019) and fluxes for faults and fractures were accordingly calculated. However, fluid velocity within fractures and faults generated by injection and production scenarios was dramatically higher than the induced velocity by the background convective flux. Consequently, the influence of this natural flux on the produced tracer concentration at GPK2 is negligible (Fig. 9a), and ignoring this factor causes an increase of about 2% in the concentration for GPK2. For GPK4, the background flow is opposing the available hydraulic gradient and thus lowers the recorded tracer concentrations by around 5% at the end of the tracer experiment (Fig. 9b).

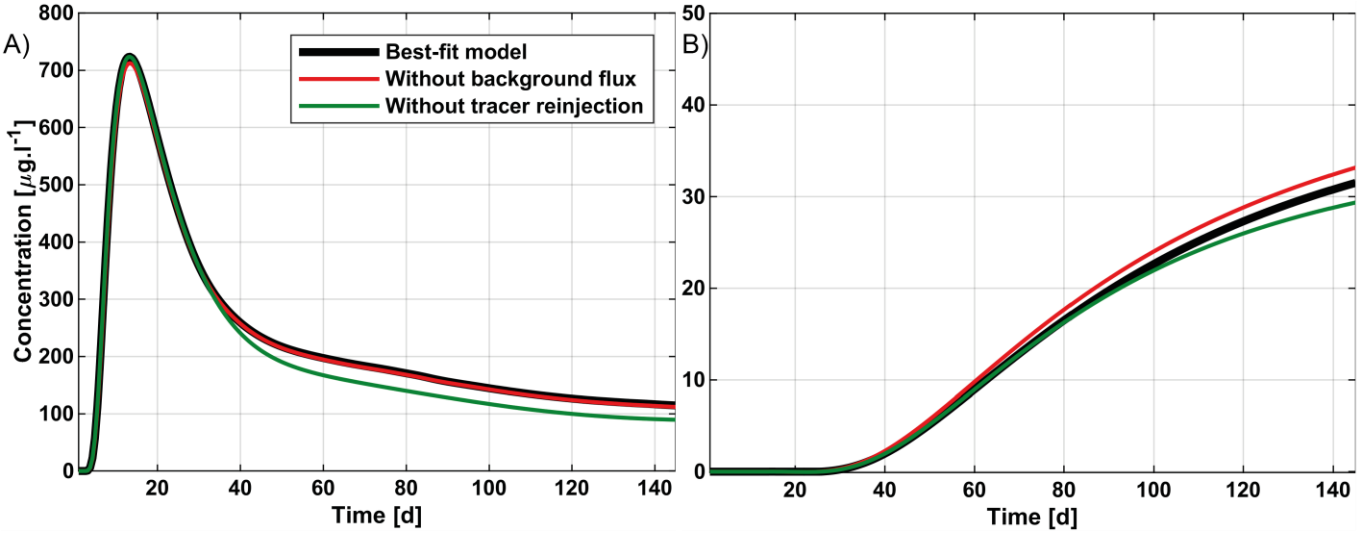

Fig. 9: Sensitivity of concentration due to background flux and tracer reinjection of the wells GPK2 (A) and GPK4 (B). Note the different axis scale.

5. Discussion

Our results, therefore, confirm the existence of different pathways, connecting the wells of the Soultz geothermal reservoir along different faults and fractures. The wells GPK3 and GPK2 show a good and fast hydraulic connection, which is realized by three different pathways with different travel and residence times. Low measurable tracer concentrations indicate a poor hydraulic connection between GPK3 and GPK4. The convective background flux, as proposed by Sanjuan et al. (2006),

has a minor effect on the resulting concentrations, as the forced fluid velocities exceed the natural convective velocities by several orders of magnitude.

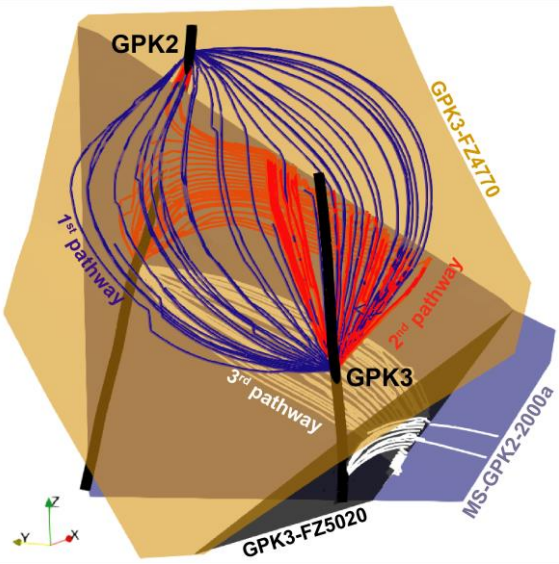

Fig. 10: The main fractures and flow paths connecting the wells GPK3 and GPK2. The first pathway connects both wells along GPK3-FZ4770, the second pathway along GPK3-FZ4770 and MS-GPK2-2000a and the third pathway along GPK3-FZ5020 and MS-GPK2-2000a. The streamlines are displayed for visualizing the fracture flow.

As shown in Fig. 9, re-circulated brine, containing tracers, can lead to a significant long-term increase in the overall concentration and it should be considered in momentum analysis of tracer recovery, swept volume and heat exchange area (Shook, 2005). The cumulative tracer recovery ratio, R_{fluo}, is the sum of the recovered solutes of each pathway (Fig. 6). It can be calculated from the time-concentration plot by multiplying the concentration data with the production flow rate and the inverse of the totally injected tracer-mass. As calculated in Table 3, the total tracer recovery during the experimental period is 25.0 %, which GPK2 and GPK4 contributed 24.6 % and 0.4 %, respectively. The total recovery of the model presented is well comparable with the experimental data and the extrapolated results from it (23.5 % (Sanjuan et al., 2006) and 25.3 % (Sanjuan et al., 2015)) although the individual contributions are not exactly matched. The stronger influence of the second pathway for GPK2 in the numerical simulation is partly caused by the slight overestimation after 78 days as demonstrated in Fig. 6. The overestimation of the long-term values can have various causes. One possible reason are unknown fractures, which are hydraulically connected to the second pathway. Such fractures could not be considered in the model, because they were not drilled and therefore neither their geometric appearance nor their hydraulic influence on the reservoir are known (Mégel et al., 2005). Another explanation of the slight differences can be the connection of the two fractures since its internal structure is unknown, but complex flow pattern and thus mixing processes can occur here (Berkowitz et al., 1994). The neglected thermal decay of the fluorescein can also lead to slight deviations in the results, especially over a longer period of time (Adams and Davis, 1991). On the other hand, considering tracer diffusion into the matrix can increase the long-term concentration results, while the peak is lowered (Ghergut et al., 2018). This simplification is

nevertheless permissible since there is no evidence of matrix diffusion (Radilla et al., 2012) and the system is strongly convective, with the time scale of the transport process being significantly shorter than that of the diffusion into the matrix (Bodin et al., 2003).

The swept volume can be calculated from the recovery rate. The swept volume, V_{swept}, is a measure of the pore volume swept by tracer during an experiment as (Levenspiel 1972):

$$V_{swept} = \mathrm{q}_{inj} * \tau * \mathrm{R}_{fluo} \qquad \text{Eq. 4}$$

where τ is the mean residence time, corrected for the tracer recycling and q_{inj} is the injection rate. Key assumptions for these calculations are a steady flow field on the affected fractures and the usage of a conservative tracer without mass losses. The swept or pore volume for the connection of GPK3 and GPK2 is 4000 m³ for the first pathway and 10300 m³ for the second pathway. The swept volume for the first pathway and Sanjuan et al. (2006) are a perfect match, while the value of the second pathway is rising by around 60 %, which is due to the higher recovery rate in simulations. If a mean transfer time for GPK4 is calculated at the end of the experiment (145 days), the total swept volume is 133 m³, which corresponds to Sanjuan et al. (2006). However, it is significantly smaller compared to the main pathways between GPK3 and GPK2.

Table 3: Summary of the recovery ratio and swept pore volume of the inter-well flow between GPK3 - GPK2 and GPK3 - GPK4 as resulting from recovered solute concentrations in comparison to Sanjuan et al. (2006)

Wells	$\mathbf{R}_{fluo}$ **[%]**		$\boldsymbol{V}_{swept}$ **[m³]**	
	This study	Sanjuan et al. (2006)	This study	Sanjuan et al. (2006)
GPK2 – 1st pathway	14.5	15.6	4000	3900
GPK2 – 2nd pathway	10.1	7.9	10300	6500
GPK4	0.4	1.8	133	120
Total	25.0	25.3	14533	10520

The results confirm the existence of a fractured zone between the wells GPK3 and GPK4. After calibration of the numerical model using hydraulic and tracer tests, the Separation fracture, which is oriented WNW-ESE, could be assigned as a hydraulic conduit between the NNW-SSE striking fractures. The fracture is connecting the northern reservoir with the main fault system and creating a preferential fluid pathway. Since the fractures intersecting GPK4 (MS-GPK4-20045b and GPK4-FZ4710) have a higher resistance to fluid flow than the Separation fracture, the tracer is mainly transported and mixed along this fracture and only little amount passes to the southern reservoir and GPK4. The results are in agreement with the microseismic inversion of Kohl et al. (2006), which indicated a seismically inactive E-W-striking plane that could be either highly permeable or totally sealed. Calò et al. (2016) concluded a seismic anomalous zone between the two wells from Vertical Seismic Profiling as well. Barton et al. (1995) observed that fractures oriented perpendicular to the maximum horizontal stress have a higher probability to be sealed. Here, the fracture possesses a

high hydraulic conductivity, even as the orientation is unfavorable in terms of dilation with respect to the regional stress field. Localized stress perturbations and a transition in the stress regime (from normal-faulting to strike-slip) are known for the deepest parts of the Soultz reservoir (Cuenot et al., 2006; Dorbath et al., 2010). Comparable observations could also be made for the nearby Bruchsal geothermal power plant. Several antithetic fractures have been detected, which are misaligned with the recent stress field and are a result of the complex tectonic history of the URG (Meixner et al., 2016). Those misoriented fault zones can, as indicated in this study, have an impact on the local flow field.

In the northern part of the reservoir, the fracture GPK3-FZ4770 creates the shortest pathway between the wells GPK3 and GPK2, with the main contribution to the inter-well flow and an average fluid velocity of 2.6 $m.h^{-1}$. As the breakthrough curve is completely captured within the experimental time, the minimum heat exchange area for this pathway can be calculated. The minimal heat exchange surface area is the area of the fracture surfaces swept by fluid traveling from the injection to the production well assuming a parallel plate model with the known pore volume and aperture (Robinson and Tester, 1984). The area along the GPK3-FZ4770, which was analytically calculated from the pore volume swept ($1.1x10^6$ m^2), is half of the area ($2.1x10^6$ m^2) determined by the analysis of the streamlines between the wells in the simulation results (Fig. 10). In reality, the heat exchange area tends to be even higher due to the complex internal structure of fractures, which is simplified in the model. Fractures in the area of Soultz are typically described as zones of highly clustered shear fractures with varying aperture and length. A core zone is surrounded by a damage zone and hydrothermally altered granite (Dezayes et al., 2010). Shook (2003) developed a concept for quantifying the relationship between the flow capacity of the set of fracture channels and its storage capacity. According to this approach, the fracture GPK3-FZ4770 can be described as a set of clustered channels with non-uniform internal structure in which half of the fluid produced in the experiments passes through 27 % of the pore volume. Therefore, the heat surface area, where the exchange between the fracture and the matrix occurs, tends to be larger than calculated and simulated with the parallel plate approach. The flow field along the fracture is asymmetric. As already shown in Fig. 8, most of the fluids recovered in GPK2 originated from a relatively small area between the two boreholes. However, a great amount of the injected solute remained in deeper sections of the reservoir and the fracture GPK3-FZ4770 without ever entering the influence region of GPK2. Detailed quantification of the minimal heat exchange area for the second and third pathways, as shown in Fig. 8 is not possible as the flow and the inter-well connection occur at a set of fractures with different flow velocities and residence times, and time-concentration plot (Fig. 6) shows ongoing recovery beyond the end of the experiment. The same issues also apply to the connection between GPK3 and GPK4.

The new results of the deep connection of the GPK2, GPK3 and GPK4 wells allow the reassessment of the performance of the Soultz-sous-Forêts heat exchanger system. The recalibration of the hydraulic model points to rapid fluid pathways in the central-northern part of the reservoir (between GPK1 and GPK2) increasing the risk of a (thermal) breakthrough. In contrast, for the operating scheme used in the tracer experiment, short circuits are rather unlikely due to the connection to the large-scale circulation system. The same applies to the current economic operation, where reservoir brine is produced from GPK2 and reinjected into GPK3 and GPK4 wells (Mouchot et al., 2018). Moreover, it could be shown that the northernmost part of the deep reservoir (north of GPK2), as well as the connection of the separation fracture to the regional fault system, has enlarged hydraulic conductivity and thus could potentially be the target for future research and exploration. The hydraulic model presented here can be used as a basis for the design and prediction of future experiments.

6. Conclusion

In the past, many attempts have been made to describe the flow field in the Soultz geothermal reservoir. Mostly, the individual interconnections of the wells were considered separately, while a holistic and more general description of the reservoir pathways often failed. In this paper, the developed and presented concept allows the simultaneous matching of the tracer's breakthrough curves on both production wells and the qualitative and quantitative identification of the different hydraulic interconnections along the fault and fracture network based on the structural model of the Soultz reservoir.

The Soultz EGS can be described as a fractured reservoir connecting different wells along flow channels generated by the main hydraulic pathways. The hydraulic connection of GPK3 and GPK2 was established along highly transmissive pathways with two fluorescein peak times of 13 and 90 days. The main direct pathway is occurring along the fracture GPK3-FZ4770, which accounts for 14.5 % of the tracer contribution. The cumulative tracer recovery of the different pathways is 25 % while the total swept volume is 14533 m^3. The minimal heat exchanger surface on the main pathway is 2.1×10^6 m^2. The value is twice as large as the expected value from the analytical evaluation of the experiment. In contrast, the connection between GPK3 and GPK4 has no directly identifiable fluid pathway. The forecast modeling predicted a peak arrival after 1.5 years of continuous injection with the maximum tracer concentration which is 10 times lower than for GPK2. Only a small amount of tracer is recovered from the well GPK4 (0.4 %), and the swept pore volume is approximately two orders of magnitude smaller (133 m^3) than the direct and well-established connection of GPK2. The impeded connection between GPK3 and GPK4 is presumably related to a WNW-ESE-oriented fractured zone, establishing a preferential fluid pathway, connecting the northern reservoir with the local fault network, while the southern reservoir is only connected by minor transmissive fractures to this conductive zone. According to the new hydraulic model, further

exploration and experimental research should focus on the connection of the Soultz geothermal reservoir to the regional fault network.

Acknowledgments

We thank the anonymous reviewers for their constructive criticisms that helped to improve the quality of the manuscript. The authors acknowledge the financial support by the Federal Ministry for Economic Affairs and Energy of Germany in the project GeoFaces (No. 0324025C) and the Helmholtz portfolio project “Geoenergy”. The support from the program “Renewable Energies”, under the topic “Geothermal Energy Systems”, is gratefully acknowledged. We also thank the EnBW Energie Baden-Württemberg AG for supporting geothermal research at KIT.

References

Adams, M.C., Davis, J., 1991. Kinetics of fluorescein decay and its application as a geothermal tracer. Geothermics 20 (1-2), 53–66. doi:10.1016/0375-6505(91)90005-G.

Aichholzer, C., Duringer, P., Orciani, S., Genter, A., 2016. New stratigraphic interpretation of the Soultz-sous-Forêts 30-year-old geothermal wells calibrated on the recent one from Rittershoffen (Upper Rhine Graben, France). Geotherm Energy 4 (1), 132. doi:10.1186/s40517-016-0055-7.

Aquilina, L., Dreuzy, J.-R. de, Bour, O., Davy, P., 2004. Porosity and fluid velocities in the upper continental crust (2 to 4 km) inferred from injection tests at the Soultz-sous-Forêts geothermal site. Geochimica et Cosmochimica Acta 68 (11), 2405–2415. doi:10.1016/j.gca.2003.08.023.

Aquilina, L., Rose, P., Brach, M., Gentier, S., Jeannot, R., Jacquot, E., Audigane, P., Tran-Vie, T., Jung, R., Baumgärtner, J., Baria, R., Gérard, A., 1998. A Tracer Test at the Soultz-Sous-Forêts Hot Dry Rock Geothermal Site: PROCEEDINGS, Twenty-Third Workshop on Geothermal Reservoir Engineering, Stanford, California, 8 pp.

Ayling, B.F., Hogarth, R.A., Rose, P.E., 2016. Tracer testing at the Habanero EGS site, central Australia. Geothermics 63, 15–26. doi:10.1016/j.geothermics.2015.03.008.

Bächler, D., Kohl, T., Rybach, L., 2003. Impact of graben-parallel faults on hydrothermal convection—Rhine Graben case study. Physics and Chemistry of the Earth, Parts A/B/C 28 (9-11), 431–441. doi:10.1016/S1474-7065(03)00063-9.

Barton, C.A., Zoback, M.D., Moos, D., 1995. Fluid flow along potentially active faults in crystalline rock. Geol 23 (8), 683. doi:10.1130/0091-7613(1995)023<0683:FFAPAF>2.3.CO;2.

Bataillé, A., Genthon, P., Rabinowicz, M., Fritz, B., 2006. Modeling the coupling between free and forced convection in a vertical permeable slot: Implications for the heat production of an Enhanced Geothermal System. Geothermics 35 (5-6), 654–682. doi:10.1016/j.geothermics.2006.11.008.

Bauget, F., Fourar, M., 2007. Convective dispersion in a real fracture: PROCEEDINGS: Thirty-Second Workshop on Geothermal Reservoir Engineering Stanford University, Stanford, California, 8 pp.

Baujard, C., Bruel, D., 2006. Numerical study of the impact of fluid density on the pressure distribution and stimulated volume in the Soultz HDR reservoir. Geothermics 35 (5-6), 607–621. doi:10.1016/j.geothermics.2006.10.004.

Bear, J., Cheng, A.H.-D., 2010. Modeling Groundwater Flow and Contaminant Transport. Theory and Applications of Transport in Porous Media 23. Springer Science+Business Media B.V, Dordrecht. doi:10.1007/978-1-4020-6682-5.

558 Becker, M.W., Shapiro, A.M., 2000. Tracer transport in fractured crystalline rock: Evidence of
559 nondiffusive breakthrough tailing. Water Resour. Res. 36 (7), 1677–1686.
560 doi:10.1029/2000WR900080.

561 Berkowitz, B., 2002. Characterizing flow and transport in fractured geological media: A review.
562 Advances in Water Resources 25 (8-12), 861–884. doi:10.1016/S0309-1708(02)00042-8.

563 Berkowitz, B., Naumann, C., Smith, L., 1994. Mass transfer at fracture intersections: An evaluation
564 of mixing models. Water Resour. Res. 30 (6), 1765–1773. doi:10.1029/94WR00432.

565 Berre, I., Doster, F., Keilegavlen, E., 2018. Flow in Fractured Porous Media: A Review of Conceptual
566 Models and Discretization Approaches. Transp Porous Med 137 (02), 49. doi:10.1007/s11242-
567 018-1171-6.

568 Blumenthal, M., Kühn, M., Pape, H., Rath, V., Clauser, C., 2007. Hydraulic model of the deep
569 reservoir quantifying the multi-well tracer test. Paper presented at EHDRA Scientific Conference,
570 28-29 June 2007.

571 Bodin, J., Delay, F., Marsily, G. de, 2003. Solute transport in a single fracture with negligible matrix
572 permeability: 1. fundamental mechanisms. Hydrogeology Journal 11 (4), 418–433.
573 doi:10.1007/s10040-003-0268-2.

574 Brooks, A.N., Hughes, T.J.R., 1982. Streamline upwind/Petrov-Galerkin formulations for convection
575 dominated flows with particular emphasis on the incompressible Navier-Stokes equations.
576 Computer Methods in Applied Mechanics and Engineering 32 (1-3), 199–259. doi:10.1016/0045-
577 7825(82)90071-8.

578 Bundschuh, J., Suárez Arriaga, M.C., Arriaga, M.C.S., Suárez-Arriaga, M.C., 2010. Introduction to
579 the numerical modeling of groundwater and geothermal systems: Fundamentals of mass, energy,
580 and solute transport in poroelastic rocks. Multiphysics modeling 2. CRC Press, Boca Raton Fla.
581 u.a., XLII, 479 S.

582 Calò, M., Dorbath, C., Lubrano Lavadera, P., 2016. Can faults become barriers for deep fluid
583 circulation? Insights from high-resolution seismic VSP tomography at the Soultz-sous-Forêts
584 geothermal site. Geophys. Res. Lett 43 (17), 8986–8993. doi:10.1002/2016GL069623.

585 Cornet, F.H., Bérard, T., Bourouis, S., 2007. How close to failure is a granite rock mass at a 5km
586 depth? International Journal of Rock Mechanics and Mining Sciences 44 (1), 47–66.
587 doi:10.1016/j.ijrmms.2006.04.008.

588 Crank, J., Nicolson, P., 1996. A practical method for numerical evaluation of solutions of partial
589 differential equations of the heat-conduction type. Adv Comput Math 6 (1), 207–226.
590 doi:10.1007/BF02127704.

591 Cuenot, N., Charléty, J., Dorbath, L., Haessler, H., 2006. Faulting mechanisms and stress regime at
592 the European HDR site of Soultz-sous-Forêts, France. Geothermics 35 (5-6), 561–575.
593 doi:10.1016/j.geothermics.2006.11.007.

594 Dezayes, C., Genter, A., Valley, B., 2010. Structure of the low permeable naturally fractured
595 geothermal reservoir at Soultz. Comptes Rendus Geoscience 342 (7-8), 517–530.
596 doi:10.1016/j.crte.2009.10.002.

597 Dorbath, L., Evans, K., Cuenot, N., Valley, B., Charléty, J., Frogneux, M., 2010. The stress field at
598 Soultz-sous-Forêts from focal mechanisms of induced seismic events: Cases of the wells GPK2
599 and GPK3. Comptes Rendus Geoscience 342 (7-8), 600–606. doi:10.1016/j.crte.2009.12.003.

600 Evans, J.P., Forster, C.B., Goddard, J.V., 1997. Permeability of fault-related rocks, and implications
601 for hydraulic structure of fault zones. Journal of Structural Geology 19 (11), 1393–1404.
602 doi:10.1016/S0191-8141(97)00057-6.

603 Fox, D.B., Sutter, D., Beckers, K.F., Lukawski, M.Z., Koch, D.L., Anderson, B.J., Tester, J.W., 2013.
604 Sustainable heat farming: Modeling extraction and recovery in discretely fractured geothermal
605 reservoirs. Geothermics 46, 42–54. doi:10.1016/j.geothermics.2012.09.001.

606 Garnish, J., 2002. European activities in Hot Dry Rock research. Open Meeting on Enhanced
607 Geothermal Systems, 8–9.

608 Gaston, D., Newman, C., Hansen, G., Lebrun-Grandié, D., 2009. MOOSE: A parallel computational
609 framework for coupled systems of nonlinear equations. Nuclear Engineering and Design 239
610 (10), 1768–1778. doi:10.1016/j.nucengdes.2009.05.021.

611 Genter, A., Baujard, C., Cuenot, N., Dezayes, C., Kohl, T., Masson, F., Sanjuan, B., Scheiber, J.,
612 Schill, E., Schmittbuhl, J., Vidal, J., 2016. Geology, Geophysics and Geochemistry in the Upper
613 Rhine Graben: the frame for geothermal energy use. European Geothermal Congress 2016,
614 5 pp.

615 Genter, A., Cuenot, N., Goerke, X., Moeckes, W., Scheiber, J., 2011. Scientific and technical activity
616 of the Soultz geothermal power plant, Progress report from December 2010 to June 2011: GEIE
617 report RA05 002, 59 pp.

618 Genter, A., Evans, K., Cuenot, N., Fritsch, D., Sanjuan, B., 2010. Contribution of the exploration of
619 deep crystalline fractured reservoir of Soultz to the knowledge of enhanced geothermal systems
620 (EGS). Comptes Rendus Geoscience 342 (7-8), 502–516. doi:10.1016/j.crte.2010.01.006.

621 Gentier, S., Rachez, X., Ngoc, T.D.T., Peter-Borie, M., Souque Christine, 2010. 3D Flow Modelling
622 of the Medium-Term Circulation Test Performed in the Deep Geothermal Site of Soultz-Sous-
623 forêts (France): PROCEEDINGS World Geothermal Congress 2010, Bali, Indonesia, 13 pp.

624 Gentier, S., Rachez, X., Peter-Borie, M., Blaisonneau, A., Sanjuan, B., 2011. Transport and Flow
625 Modelling of the Deep Geothermal Exchanger Between Wells at Soultz-sous-Forêts (France).
626 GRC Transactions 35, 363–369.

627 Gérard, A., Genter, A., Kohl, T., Lutz, P., Rose, P., Rummel, F., 2006. The deep EGS (Enhanced
628 Geothermal System) project at Soultz-sous-Forêts (Alsace, France). Geothermics 35 (5-6), 473–
629 483. doi:10.1016/j.geothermics.2006.12.001.

630 Gessner, K., Kühn, M., Rath, V., Kosack, C., Blumenthal, M., Clauser, C., 2009. Coupled Process
631 Models as a Tool for Analysing Hydrothermal Systems. Surv Geophys 30 (3), 133–162.
632 doi:10.1007/s10712-009-9067-1.

633 Ghergut, I., Behrens, H., Sauter, M., Licha, T., Nottebohm, M., 2013. Can Peclet numbers depend
634 on tracer species? going beyond SW test insensitivity to advective or equilibrium-exchange
635 processes.: PROCEEDINGS, Thirty-Eighth Workshop on Geothermal Reservoir Engineering,
636 Stanford, California, 10 pp.

637 Ghergut, J., Behrens, H., Bansabat, J., Sauter, M., Wagner, B., Wiegand, B., 2018. Sorption, matrix
638 diffusion, … need not make a major difference for frac characterization from short-term tracer
639 signals: PROCEEDINGS, 43rd Workshop on Geothermal Reservoir Engineering,
640 Stanford, California, 13 pp.

641 Ghergut, J., Behrens, H., Sauter, M., 2016. Petrothermal and aquifer-based EGS in the Northern-
642 German Sedimentary Basin, investigated by conservative tracers during single-well injection-
643 flowback and production tests. Geothermics 63, 225–241.
644 doi:10.1016/j.geothermics.2016.01.015.

645 Gholami Korzani, M., Held, S., Kohl, T., 2019. Numerical based filtering concept for feasibility
646 evaluation and reservoir performance enhancement of hydrothermal doublet systems.
647 Submitted. Journal of Petroleum Science and Engineering.

648 Guillou-Frottier, L., Carrė, C., Bourgine, B., Bouchot, V., Genter, A., 2013. Structure of hydrothermal
649 convection in the Upper Rhine Graben as inferred from corrected temperature data and basin-
650 scale numerical models. Journal of Volcanology and Geothermal Research 256, 29–49.
651 doi:10.1016/j.jvolgeores.2013.02.008.

652 Hadermann, J., Heer, W., 1996. The Grimsel (Switzerland) migration experiment: integrating field
653 experiments, laboratory investigations and modelling. Journal of Contaminant Hydrology 21 (1-
654 4), 87–100. doi:10.1016/0169-7722(95)00035-6.

655 Held, S., Genter, A., Kohl, T., Kölbel, T., Sausse, J., Schoenball, M., 2014. Economic evaluation of
656 geothermal reservoir performance through modeling the complexity of the operating EGS in
657 Soultz-sous-Forêts. Geothermics 51, 270–280. doi:10.1016/j.geothermics.2014.01.016.

658 Hettkamp, T., Fuhrmann, G., Rummel, F., 1999. Hydraulic properties of the Rheingraben basement
659 material. Bulletin d'Hydrogiologie No 17.

660 Hooijkaas, G.R., Genter, A., Dezayes, C., 2006. Deep-seated geology of the granite intrusions at
661 the Soultz EGS site based on data from 5km-deep boreholes. Geothermics 35 (5-6), 484–506.
662 doi:10.1016/j.geothermics.2006.03.003.

663 Iglesias, E.R., Flores-Armenta, M., Torres, R.J., Ramirez-Montez, M., Reyes-Picaso, N., Cruz-
664 Grajales, I., 2015. Tracer Testing at Los Humeros, Mexico, High-Enthalpy Geothermal Field:
665 PROCEEDINGS World Geothermal Congress 2015, Melbourne, 8 pp.

666 Jung, R., Schindler, M., Nami, P., Tischner, T., 2010. Determination of flow exits in the Soultz
667 borehole GPK2 by using the brine displacement method. Comptes Rendus Geoscience 342 (7-
668 8), 636–643. doi:10.1016/j.crte.2009.06.002.

669 Karmakar, S., Ghergut, J., Sauter, M., 2016. Early-flowback tracer signals for fracture
670 characterization in an EGS developed in deep crystalline and sedimentary formations: a
671 parametric study. Geothermics 63, 242–252. doi:10.1016/j.geothermics.2015.08.007.

672 Kestin, J., Khalifa, H.E., Correia, R.J., 1981. Tables of the dynamic and kinematic viscosity of
673 aqueous KCl solutions in the temperature range 25–150 °C and the pressure range 0.1–35 MPa.
674 Journal of Physical and Chemical Reference Data 10 (1), 57–70. doi:10.1063/1.555640.

675 Kohl, T., Bächler, D., Rybach, L., 2000. Steps towards a comprehensive thermo-hydraulic analysis
676 of the HDR test site Soultz-sous-Forêts. Proc. World Geothermal Congress, 3459–3464.

677 Kohl, T., Baujard, C., Mégel, T., 2006. Conditions for mechanical re-stimulation of GPK4. Paper
678 presented at EHDRA Scientific Conference, 15-16 June 2006.

679 Kohl, T., Mégel, T., 2007. Predictive modeling of reservoir response to hydraulic stimulations at the
680 European EGS site Soultz-sous-Forêts. International Journal of Rock Mechanics and Mining
681 Sciences 44 (8), 1118–1131. doi:10.1016/j.ijrmms.2007.07.022.

682 Kosack, C., Vogt, C., Rath, V., Marquart, G., 2011. Stochastic Estimates of the Permeability Field of
683 the Soultz-sous-Forêts Geothermal Reservoir - Comparison of Bayesian Inversion, MC
684 Geostatistics, and EnKF Assimilation: PROCEEDINGS, Thirty-Sixth Workshop on Geothermal
685 Reservoir Engineering, Stanford.

686 Mégel, T., Kohl, T., Gérard, A., Rybach, L., Hopkirk, R., 2005. Downhole Pressures Derived from
687 Wellhead Measurements during Hydraulic Experiments: PROCEEDINGS World
688 Geothermal Congress 2005, Antalya, Turkey, 6 pp.

689 Meixner, J., Schill, E., Grimmer, J.C., Gaucher, E., Kohl, T., Klingler, P., 2016. Structural control of
690 geothermal reservoirs in extensional tectonic settings: An example from the Upper Rhine Graben.
691 Journal of Structural Geology 82, 1–15. doi:10.1016/j.jsg.2015.11.003.

692 Moreno, L., Tsang, Y.W., Tsang, C.F., Hale, F.V., Neretnieks, I., 1988. Flow and tracer transport in
693 a single fracture: A stochastic model and its relation to some field observations. Water Resour.
694 Res. 24 (12), 2033–2048. doi:10.1029/WR024i012p02033.

695 Mouchot, J., Genter, A., Cuenot, N., Scheiber, J., Seibel, O., Bosia, C., Ravier, G., 2018. First Year
696 of Operation from EGS geothermal Plants in Alsace, France: Scaling Issues: PROCEEDINGS,
697 43rd Workshop on Geothermal Reservoir Engineering, 12 pp.

698 O'Sullivan, M.J., Pruess, K., Lippmann, M.J., 2001. State of the art of geothermal reservoir
699 simulation. Geothermics 30 (4), 395–429. doi:10.1016/S0375-6505(01)00005-0.

700 Pfender, M., Nami, P., Tischner, T., Jung, R., 2006. Status of the Soultz deep wells based on low
701 rate hydraulic tests and temperature logs. EHDRA Scientific Conference 15.-16.06.

702 Place, J., Sausse, J., Marthelot, J.-M., Diraison, M., Géraud, Y., Naville, C., 2011. 3-D mapping of
703 permeable structures affecting a deep granite basement using isotropic 3C VSP data.
704 Geophysical Journal International 186 (1), 245–263. doi:10.1111/j.1365-246X.2011.05012.x.

705 Pribnow, D., Schellschmidt, R., 2000. Thermal tracking of upper crustal fluid flow in the Rhine
706 graben. Geophys. Res. Lett 27 (13), 1957–1960. doi:10.1029/2000GL008494.

707 Radilla, G., Sausse, J., Sanjuan, B., Fourar, M., 2012. Interpreting tracer tests in the enhanced
708 geothermal system (EGS) of Soultz-sous-Forêts using the equivalent stratified medium
709 approach. Geothermics 44, 43–51. doi:10.1016/j.geothermics.2012.07.001.

710 Robinson, B.A., Tester, J.W., 1984. Dispersed fluid flow in fractured reservoirs: An analysis of tracer-
711 determined residence time distributions. J. Geophys. Res. Solid Earth 89 (B12), 10374–10384.
712 doi:10.1029/JB089iB12p10374.

713 Rose, P., Leecaster, K., Drakos, P., Robertson-Tait, A., 2009. Tracer Testing at the Desert Peak
714 EGS Project. GRC Transactions 33, 241–249.

715 Sanjuan, B., Brach, M., Genter, A., Sanjuan, R., Scheiber, J., Touzelet, S., 2015. Tracer testing of
716 the EGS site at Soultz-sous-Forêts (Alsace, France) between 2005 and 2013: Proceedings World
717 Geothermal Congress 2015, Melbourne, 12 pp.

718 Sanjuan, B., Pinault, J.-L., Rose, P., Gérard, A., Brach, M., Braibant, G., Crouzet, C., Foucher, J.-
719 C., Gautier, A., Touzelet, S., 2006. Tracer testing of the geothermal heat exchanger at Soultz-
720 sous-Forêts (France) between 2000 and 2005. Geothermics 35 (5-6), 622–653.
721 doi:10.1016/j.geothermics.2006.09.007.

722 Sausse, J., Dezayes, C., Dorbath, L., Genter, A., Place, J., 2010. 3D model of fracture zones at
723 Soultz-sous-Forêts based on geological data, image logs, induced microseismicity and vertical
724 seismic profiles. Comptes Rendus Geoscience 342 (7-8), 531–545.
725 doi:10.1016/j.crte.2010.01.011.

726 Sausse, J., Genter, A., 2005. Types of permeable fractures in granite. Geological Society, London,
727 Special Publications 240 (1), 1–14. doi:10.1144/GSL.SP.2005.240.01.01.

728 Schill, E., Genter, A., Cuenot, N., Kohl, T., 2017. Hydraulic performance history at the Soultz EGS
729 reservoirs from stimulation and long-term circulation tests. Geothermics 70, 110–124.
730 doi:10.1016/j.geothermics.2017.06.003.

731 Schindler, M., 2009. Hydraulic Data recorded during the three circulations with down-hole pumps at
732 soultz, Rapport Public GEIE n◦ RAP 71 000 V00. GEIE, Soultz-sous-Forêts, France,, 20 pp.

733 Schindler, M., Baumgärtner, J., Gandy, T., Hauffe, P., Hettkamp, T., Menzel, H., Penzkofer, P., Teza,
734 D., Tischner, T., Wahl, G., 2010. Successful Hydraulic Stimulation Techniques for Electric Power
735 Production in the Upper Rhine Graben, Central Europe: PROCEEDINGS World Geothermal
736 Congress 2010, Bali, Indonesia, 7 pp.

737 Schmittbuhl, J., Steyer, A., Jouniaux, L., Toussaint, R., 2008. Fracture morphology and viscous
738 transport. International Journal of Rock Mechanics and Mining Sciences 45 (3), 422–430.
739 doi:10.1016/j.ijrmms.2007.07.007.

740 Shook, G.M., 2003. A simple, fast method of estimating fractured reservoir geometry from tracer
741 tests. GRC Transactions (27), 407–411.

742 Shook, G.M., 2005. A systematic method for tracer test analysis: An example using Beoware tracer
743 data: PROCEEDINGS, Thirtieth Workshop on Geothermal Reservoir Engineering,
744 Stanford, California, 6 pp.

745 Stober, I., Bucher, K., 2007. Hydraulic properties of the crystalline basement. Hydrogeol J 15 (2),
746 213–224. doi:10.1007/s10040-006-0094-4.

747 Tsang, Y.W., Tsang, C.F., Neretnieks, I., Moreno, L., 1988. Flow and tracer transport in fractured
748 media: A variable aperture channel model and its properties. Water Resour. Res. 24 (12), 2049–
749 2060. doi:10.1029/WR024i012p02049.

750 Vallier, B., Magnenet, V., Schmittbuhl, J., Fond, C., 2019. Large scale hydro-thermal circulation in
751 the deep geothermal reservoir of Soultz-sous-Forêts (France). Geothermics 78, 154–169.
752 doi:10.1016/j.geothermics.2018.12.002.

753 Vidal, J., Genter, A., 2018. Overview of naturally permeable fractured reservoirs in the central and
754 southern Upper Rhine Graben: Insights from geothermal wells. Geothermics 74, 57–73.
755 doi:10.1016/j.geothermics.2018.02.003.

756 Vogt, C., Marquart, G., Kosack, C., Wolf, A., Clauser, C., 2012. Estimating the permeability
757 distribution and its uncertainty at the EGS demonstration reservoir Soultz-sous-Forêts using the
758 ensemble Kalman filter. Water Resour. Res. 48 (8), 393. doi:10.1029/2011WR011673.

759 Zang, A., Oye, V., Jousset, P., Deichmann, N., Gritto, R., McGarr, A., Majer, E., Bruhn, D., 2014.
760 Analysis of induced seismicity in geothermal reservoirs – An overview. Geothermics 52, 6–21.
761 doi:10.1016/j.geothermics.2014.06.005.

762 Ziegler, P.A., Dèzes, P., 2005. Evolution of the lithosphere in the area of the Rhine Rift System. Int
763 J Earth Sci (Geol Rundsch) 94 (4), 594–614. doi:10.1007/s00531-005-0474-3.